Available online at www.sciencedirect.com
SCIENCE DIRECT®
International Journal of Heat and Fluid Flow 25 (2004) 103–114
International Journal of HEAT AND FLUID FLOW
www.elsevier.com/locate/ijhff

Turbulent natural convection in an air filled partitioned square cavity

F. Ampofo *

Faculty of Engineering, Science and the Built Environment, London South Bank University, 103 Borough Road, London SE1 0AA, UK

Received 29 April 2003; accepted 22 October 2003

Abstract

An experimental study of low level turbulence natural convection in an air filled vertical partitioned square cavity was conducted. The dimensions of the cavity, which were 0.75 m high × 0.75 m wide × 1.5 m deep, resulted in 2D flow. The hot and cold walls of the cavity were isothermal at 50 and 10 °C respectively giving a Rayleigh number of 1.58×10^9. The local velocity and temperature were systematically measured at different locations in the cavity and both mean and fluctuation quantities are presented, i.e. $\overline{u}$, u'_{rms}, $\overline{v}$, v'_{rms}, $\overline{T}$, T'_{rms} and $\overline{u'v'}$. The local and average Nusselt numbers and the wall shear stress are also presented. The experiments were conducted with very high accuracy and as such the results can form experimental benchmark data and will be useful for validation of computational fluid dynamics codes.

Keywords: Natural convection; Partitions; Velocity distribution; Temperature distribution; Heat transfer; Wall shear stress; Turbulence quantities

1. Introduction

The importance of natural convection in enclosures can be found in many engineering applications such as energy transfer in rooms and buildings, nuclear reactor cooling, solar collectors and electronic equipment cooling. Natural convection in a rectangular cavity is also a very good vehicle for both experimental and theoretical studies. In experimental terms, the geometry of the rectangular cavity is simple and its boundary conditions are relatively easy to assess so that researchers can focus on the measurements of important quantities such as velocity and temperature profiles. In numerical terms, the flow phenomena in the cavity are complicated and plentiful that intrigue both physicists and engineers. However, in spite of the developments in the measurement technology and instruments, as well as in numerical methods and computers, fully describing the fluid flow and heat transfer in such a geometry still remains a challenge. In experimental studies, the flow is very sensitive to the experimental conditions. Further, boundary conditions on the horizontal cavity surfaces, defined in numerical work as adiabatic or perfectly conducting, are not easily realised in experiments, e.g. in a water filled cavity, the thermal boundary conditions on these surfaces lie somewhere in between the above two limiting cases (Nansteel and Grief, 1984). Different fluids, e.g. air and water may exhibit significantly different temperature and fluid flow patterns in cavities of similar dimensions (Olson et al., 1990). Although, convection in enclosures has been extensively studied both experimentally and numerically, only a limited number of investigators have studied partitions on the cavity walls. In addition, CFD predictions for partitioned cavities do not always compare successfully with the experimental findings. Up to now, none of the CFD codes developed can correctly predict the whole velocity and temperature fields. The discrepancy between the experimental and numerical results is obvious.

An experimental study of heat transfer and fluid flow in a multi-partitioned air filled square cavity was conducted. The objective of the study was to provide highly accurate turbulent convection data, which can provide insight into the turbulent heat transfer in natural convection in multi-partitioned enclosures and be used for the validation of computational fluid dynamics CFD codes, used in the design of electronic equipment and in the building industries. It is believed that a CFD code, which can predict the fluid flow and heat transfer in such a "congested" cavity, can be used with confidence in electronic equipment cooling studies and design optimisation.

* Tel.: +44-207-815-7013; fax: +44-207-815-7699.
E-mail address: ampofof@lsbu.ac.uk (F. Ampofo).

0142-727X/$ - see front matter © 2003 Elsevier Inc. All rights reserved.
doi:10.1016/j.ijheatfluidflow.2003.10.004

Nomenclature

A	heat transfer area (m^2)
AR_x	aspect ratio, $AR_x = H/L$
AR_z	aspect ratio for z-direction, $AR_z = D/L$
D	depth of the cavity (m)
g	gravitational acceleration (m/s^2)
h	local convective heat transfer coefficient, $h = Q/A(T_h - T_c)$ ($W/m^2\,K$)
H	height of the cavity (m)
k	thermal conductivity (W/m K)
L	width of the cavity (m)
m	any variable
n	any variable
Nu	local Nusselt number, $Nu = hL/k$
Pr	Prandtl number, $Pr = v/\alpha$
q	wall heat flux (W/m^2)
Q	rate of heat transfer (W)
Ra	Rayleigh number, $Ra = (g\beta(T_h - T_c)L^3)/\alpha v$
Ra_H	Rayleigh number based on height, $Ra_H = (g\beta(T_h - T_c)H^3)/\alpha v$
T	temperature (°C, K)
u	fluid velocity component in x-direction (m/s)
$\overline{u'v'}$	Reynolds stress (m^2/s^2)
v	fluid velocity component in y-direction (m/s)
V_o	buoyancy velocity, $V_o = \sqrt{g\beta H\Delta T}$ (m/s)
w	fluid velocity component in z-direction (m/s)
x	displacement in x-direction (m)
x, y, z	Cartesian co-ordinate
X, Y, Z	dimensionless co-ordinate
ΔT	temperature difference (K)

Greeks

α	thermal diffusivity (m^2/s)
β	thermal expansion coefficient (1/K)
μ	dynamic viscosity (kg/m s)
v	kinematic viscosity (m^2/s)
ρ	fluid density (kg/m^3)

Superscripts

–	average value
′	fluctuation component

Subscripts

b	bottom wall
c	cold wall
h	hot wall
i	arbitrary quantity
o	reference condition
t	top wall
w	wall
rms	root mean square

2. Experimental facility and procedure

The experimental facility used in the present study is depicted in Fig. 1(a). The system is fully automatically controlled and can be divided into four parts, namely the temperature control system, the cavity, and facilities for measuring the air velocity and temperature separately. The temperature control system maintained a constant temperature water flow to chambers attached to the hot and cold plates (see Fig. 1(c)). It comprised of a PC, a Schlumberger 3531F data acquisition system, a multi-loop proportional–integral–differential (PID) temperature-process controller and low noise K-type thermocouples. The computer controlled the data logging system to record the thermocouple readings and to send the signal to the PID controller. The PID controller sent pulses to the burst firing trigger modules to alter the heating power. The burst firing trigger modules switched the power on and off at zero voltage. The cold and hot water, which were controlled at predetermined temperatures, were pumped through the water chambers at a rate of 40 l/min. The test cavity, shown in Fig. 1(b) and (c), was 0.75 m high × 0.75 m wide × 1.5 m deep. In the present study, the width of the cavity, L, which happens to be equal to the height of the cavity, H, was chosen as the characteristic length scale. The hot and cold walls of the cavity were made of 6 mm mild steel plate and maintained isothermally at 50 ± 0.15 and 10 ± 0.15 °C respectively giving a Ra of 1.58×10^9. The top and bottom walls were made from 1.5 mm mild steel sheet and provided highly conducting boundaries. The temperatures on these isothermal and horizontal walls were measured using K-type thermocouples. In such a cavity, the heat loss through the passive vertical walls can be significant even when the average cavity temperature $((T_h + T_c)/2)$ is kept at the same temperature as the ambient temperature. In general,

$$q_z(x, y) = k\frac{dT}{dz} \tag{1}$$

Reducing the heat transfer on the passive vertical walls by decreasing the wall conductivity, k, is too difficult for an air filled cavity. In view of this, the only way to reduce the heat transfer on the passive vertical walls was to decrease the local temperature gradient dT/dz. For this reason, two guard cavities were mounted on each side of the working cavity (see Fig. 1(b) and (c)). A 5 mm glass sheet separated the working cavity from the

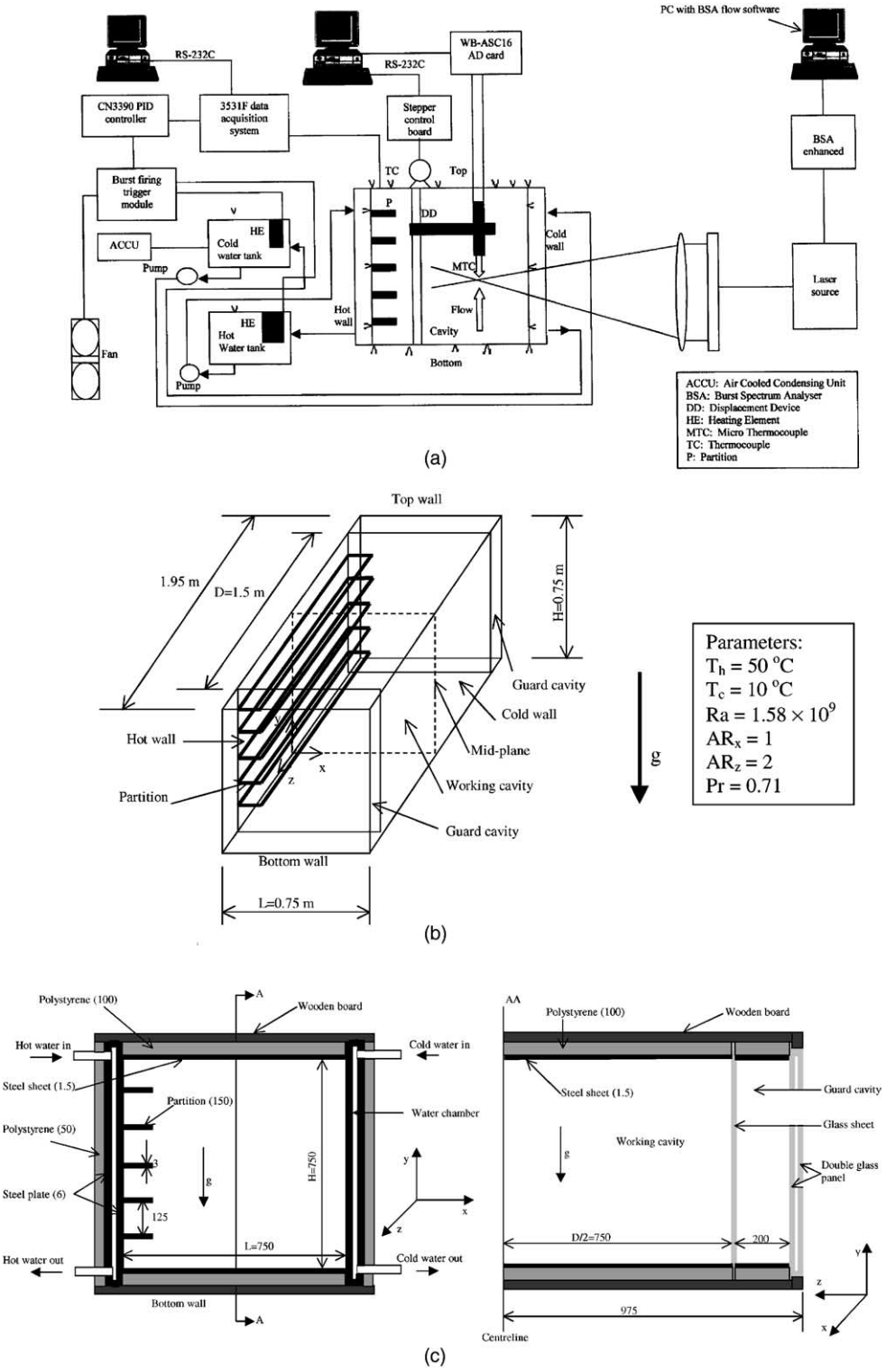

Fig. 1. Schematic diagram of the experimental facility and test cavity. (a) Experimental facility, (b) three-dimensional schematic diagram of the air filled cavity, and (c) the test cavity indicating detail of construction (all measurements are in mm).

guard cavity. Similar temperature profiles were set up on both sides of the sheet so that

$$\frac{dT}{dz} \to 0 \quad \text{and} \quad q_z(x,y) \to 0 \tag{2}$$

On the other side of the guard cavity was a double glass panel with 5 mm thick glass sheet and 10 mm gap, which reduced the heat transfer between the guard cavity and the ambient. In the present study, the ambient (room)

temperature was controlled at 30 ± 0.2 °C chosen to be equal to the cavity average temperature (average of hot and cold walls temperatures).

The partitions were 150 mm long, 1.5 m wide and made of 3 mm thick pure aluminium (1050A H22). A total of five partitions were installed on the hot wall of the cavity at 125 mm apart. The partitions were screwed on aluminium angles (25 mm × 25 mm × 1500 mm), which were in turn screwed on the hot wall. The screws heads were levelled with the angle surface and polished. Highly conductive glue was used in between the surfaces (partition surface and angle surface; angle surface and hot wall) to reduce the conduct resistance.

To measure the temperature distribution in the cavity, a micro-diameter thermocouple probe was needed to be inserted into it. A displacement device was designed to carry the probe. The requirements of the displacement device were as follows: (a) a two dimensional device that can reach all positions in one plane, (b) high location accuracy and resolution, (c) absence of or limited backlash, (d) computer controlled movement, and (e) minimum disturbance to the flow field. A schematic diagram of the displacement device is available in Ampofo (2001). In the horizontal direction (x-axis), a block moves on a twin shaft linear system. A lead screw combined with rectangular nut (M10 × 500 mm × 2 lead) is used to drive the block. In the vertical direction (y-axis), a linear guide moves on a linear guide rail. Only the linear guide rail is inserted into the cavity. At each end of the guide rail, there is a pulley. A steel wire winds over the two pulleys tightly and is connected to the linear guide. The thermocouple probe is fixed to the linear guide. The lead screw and the axis of the top pulley are connected to 1:100 gearboxes separately and these gearboxes are connected to 7.5° stepper motors. A PC controls the stepper motors through a control board. With the gearboxes and lead screw in the system, there will be a backlash when the direction is changed. This is avoided by using position switches described below. Also, the fluid flow and temperature gradient are concentrated near the vertical isothermal walls. The experimental results are more sensitive to the position in the near wall area than in the core area. This means that in the near wall area it is very important to obtain high accuracy for the thermocouple position. The measurements always started from the wall. Limit switches were used to determine the wall position. In the horizontal direction, a precision position switch (My-Com A) was installed near the thermocouple probe. According to the manufacturer, its accuracy is 10^{-3} mm. In the vertical direction, two switches (Type V4-IP67 Fully Sealed with button) were installed near the small block. According to the manufacturer, their accuracy is 10^{-1} mm.

An E type thermocouple of wire diameter 25.4 μm was carried by the computer controlled 2D displacement device (accurate to 0.1 mm) described above and was used to measure the temperature in the cavity. The response time of the 25.4 μm thermocouple is 20 Hz in still air. The choice of thermocouple was based on the experimental work of Mergui and Penot (1996), who stated that the highest turbulent frequency is less than 5 Hz in an air filled cavity ($Ra = 2.33 \times 10^9$, $AR_x = 0.9$). Thus, this thermocouple was sufficiently responsive to the high frequencies in this air cavity flow. The temperature in the cavity was read by a 16 bit data logging card (WB-ASC16 A/D card) at 50 Hz sample rate. For every location, 4096 readings were taken. In the experiments, the thermocouple probe was placed very close to the wall. The gap between the probe and the wall was reduced as much as possible. However, there was still a very small gap between the wall and the tip of the thermocouple probe. It was very difficult to put the tip of the thermocouple exactly in line with the tip of the precision position switch because of the limitation of the human eye and the flexibility of the fine wire. The gap was estimated by extrapolating the temperature fluctuation (T'_{rms}) to zero. It was found that the total error of the thermocouple probe's position was less than 0.2 mm, which included the effects of non-linear movement of the displacement device near the wall and the error in the temperature measurement. The temperature was accurate to within 0.1 K.

A back scatter, 2D LDA with a Burst Spectrum Analyser (BSA) and a 40 MHz frequency shift Bragg cell was used in the velocity measurements in the cavity. The laser source was a 300 mW argon laser. The measured velocity range was from −0.5082 to +0.5082 m/s with a resolution of 6.20E−5 m/s and at a bandwidth of 0.125 MHz. The laser beams entered the cavity through the guard cavity at an angle of 3.5° to the isothermal wall. A front lens with a focal length of 1200 mm was used. The probe volume dimensions were 0.31 mm (diameter) × 9.8 mm (length). Incense smoke was used as seeding, which lasted for more than 24 h. All measurements were started around 90 min after the incense has been burnt. This time delay was necessary to eliminate any flow disturbance caused by the burning of the incense and also to allow any disturbance, which the seeding might have introduced to decay. The LDA system had its own 3D traversing system, which was used to carry the LDA probe. Between the traverse system and the LDA probe, there was a wedge with a fixed angle of 3.5°. A small slot on the wedge can allow the probe head to move up and down through a maximum 4°. In this way, the LDA measuring point can reach all positions in the cavity, even the corners. The velocity measurement was always made from the walls. For every measuring point, either 20,000 readings were taken or the measurement lasted for 8 min. There was some blurring when the LDA probe was focused at a distance less than 0.3 mm from the wall because of the size of the LDA probe (0.31 mm). The wall position was estimated by extrapolating

the velocity to zero. It was found that the velocity distribution in the viscous sub-layer was linear and the error in the estimated wall position was less than 0.1 mm. The velocity was measured with an accuracy of 0.07%.

All the measurements were taken at the mid-plane of the cavity on a fine non-uniform mesh. During all the measurements, the experimental conditions were kept as steady as possible. Experimental repeatability was verified. The maximum deviation between readings obtained during experiments performed at different times was 0.5 K for the temperature and 2 mm/s for the velocity. For each parameter measured both the mean and fluctuation quantities were recorded. The mean, root mean square and cross-correlation quantities were calculated as follows:

The mean quantities $(\overline{T}, \bar{u}, \bar{v})$

$$\bar{m} = \frac{1}{N}\sum_{i=1}^{N} m_i \tag{3}$$

The root mean square quantities $(T'_{\mathrm{rms}}, u'_{\mathrm{rms}}, v'_{\mathrm{rms}})$

$$m'_{\mathrm{rms}} = \left[\frac{1}{N}\sum_{i=1}^{N}(m_i - \bar{m})^2\right]^{1/2} \tag{4}$$

The cross-correlation quantities $(\overline{u'v'})$

$$\overline{m'n'} = \frac{1}{N}\sum_{i=1}^{N}(m_i - \bar{m})(n_i - \bar{n}) \tag{5}$$

where N is the number of readings taken in the experiments. Up to now, most of the experimental and numerical studies were based on 2D supposition even though the real turbulent flow is 3D. In a numerical solution, 2D modelling assumes that the length in the third direction is long enough so that its influence can be neglected. However, in experiments this is not easily achieved. How deep a cavity should be for a 2D or even a quisi-2D thermal and fluid flow pattern? Penot and N'Dame (1992) pointed out that the 2D approximation of experimental natural convection in cavities should be valid if the horizontal aspect ratio (AR_z) of the cavity is greater than 1.8. In this study, AR_z was 2 and as stated earlier, there were two guard cavities on each side of the passive vertical walls. In addition, the average temperature of hot and cold walls was the same as ambient and the cavity was insulated. Hence the heat exchange between the cavity and environment was kept to a minimum. The 2D of the flow was verified by measuring the velocity distribution at $Y = y/L = 0.533$ at three different cavity planes ($Z = 0$, 0.5 and 0.8). The results are shown in Fig. 2. No obvious difference was found in the results for the flow location, which proves that the depth of the cavity, the guard cavities and the ambient of 30 °C provided a 2D flow, especially at cavity centre. The author performed an energy balance for the cavity. On

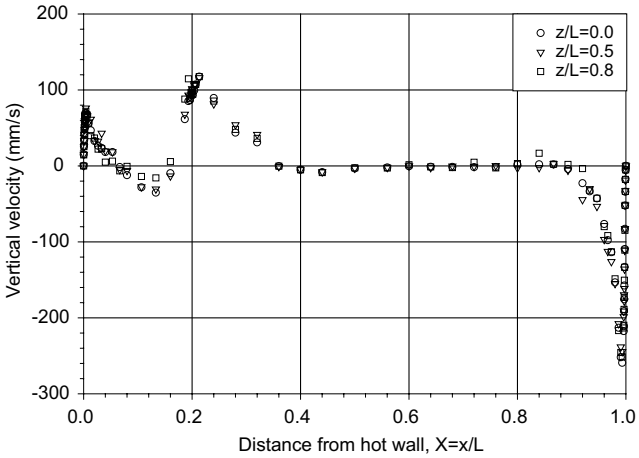

Fig. 2. Vertical velocity profile at $Y = 0.533$ and $Z = 0$, 0.5 and 0.8 (temperature measurement).

Table 1
Summary of uncertainties in the measured and estimated parameters

Parameter	Degree of uncertainty
Wall temperature	0.15 K
Air temperature	0.10 K
Air velocity	0.07%
Reynolds stress	0.10%
Rayleigh number	0.62%
Nusselt number	0.25–1.13%
Wall shear stress	1.38%

the whole, heat transfer into the cavity from the hot wall together with the partitions was 199.03 W. The net loss from the cold, bottom and top walls was 165.08, 9.88 and 20.81 W respectively. The percentage error of heat input and output in the whole cavity was 1.64%. Table 1 gives a summary of the uncertainties in the measured and estimated parameters in this study. The evaluation of the uncertainties took into account any possible uncertainties concerning positioning errors. For further details on error analysis (bias and precision errors) and propagation see Ampofo (2001).

3. Experimental results

One of the objectives of the study was to provide highly accurate turbulent convection data, which can be used for the validation of CFD codes. The experimental results, $\bar{v}$, v'_{rms}, $\bar{u}$, u'_{rms}, $\overline{T}$, T'_{rms}, $\overline{u'v'}$, at different heights of the cavity are available from the author. Figs. 3–12 show the profiles of some of the measured parameters at $Y = 0.587$ in the cavity. There is no comparable experimental or numerical past data for the present study in the partitioned cavity and as such the present data for the partitioned cavity will be compared with experimental data for standard cavity measured by the author

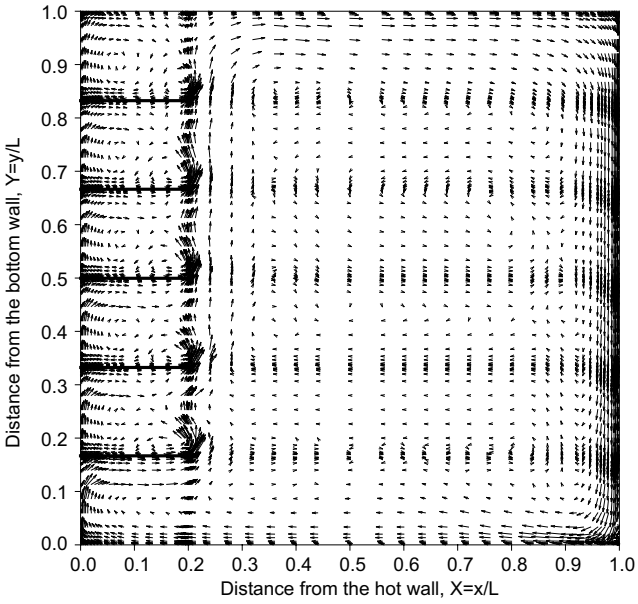

Fig. 3. Vector plot of mean velocity profiles in the partitioned cavity (scale: 0.08 m/s/mm).

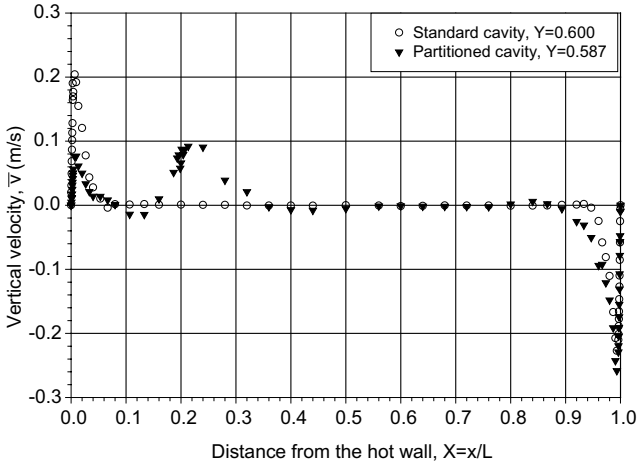

Fig. 4. Vertical velocity profile around mid-height.

in the same cavity (but without the partitions) and under the same experimental parameters and conditions (Ampofo, 2001). This will shed some light on the effect of multiple partitions on flow and thermal fields in an air filled square cavity.

3.1. Mean velocity profiles

The whole fluid flow vector plot based on all the experimental data in the partitioned cavity is shown in Fig. 3. The figure shows that the flow structure in such a congested cavity consists of boundary layer flow along all cavity walls and the partitions with flow reversal outside the cold wall and horizontal boundary layers.

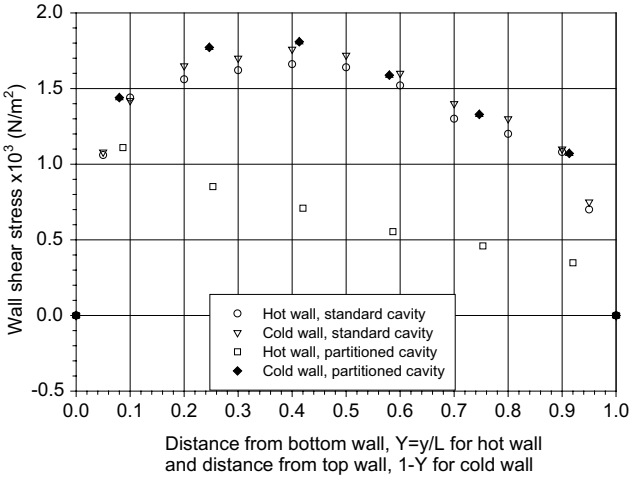

Fig. 5. Wall shear stress along the isothermal walls.

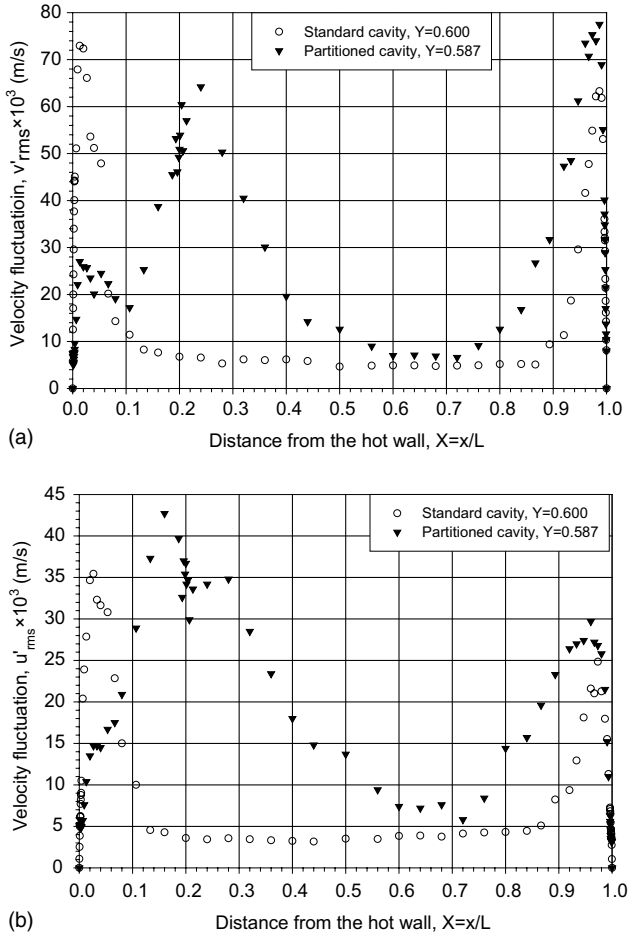

Fig. 6. Velocity fluctuation around mid-height. (a) Vertical velocity fluctuation and (b) horizontal velocity fluctuation.

In-between successive partitions, there are two vortices: one outside the boundary layer along the hot wall and the other just behind the flow in front of the partitions.

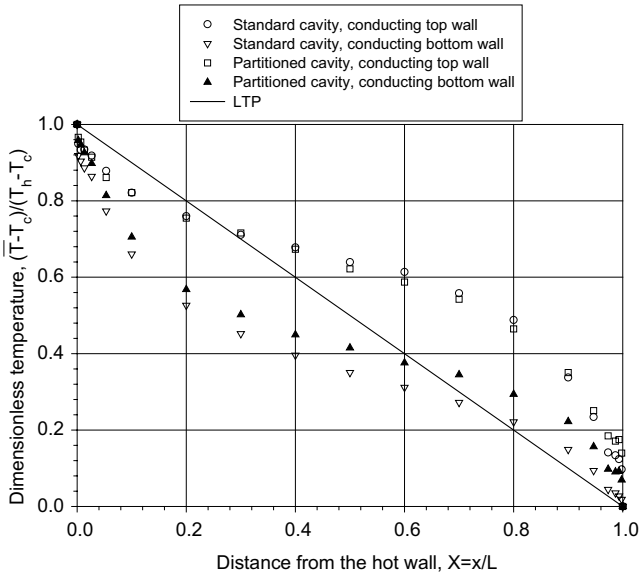

Fig. 7. Temperature profile on horizontal walls.

The vertical velocity, $\bar{v}$, profile at $Y = 0.587$ in the partitioned cavity is shown in Fig. 4. It increases steeply from the isothermal walls to a peak (with the highest peak near the cold wall) and then decreases rapidly; in some locations to slightly negative values. This means that there is rotational motion or a flow reversal at these locations. In-between successive partitions, the $\bar{v}$ then increases reaching another peak around the tip of the partitions. Away from the partitions ($X = 0.4$ and 0.8) the fluid is stationary. Fig. 4 also shows a comparison of the $\bar{v}$ profile at $Y = 0.587$ in the partitioned cavity with that in the standard cavity at $Y = 0.600$. As stated earlier, the experimental data for the standard cavity was measured by the author in the same cavity (but without the partitions) and under the same experimental parameters and conditions (Ampofo, 2001). As seen in the figure, the results in the standard cavity differ from that in the partitioned cavity especially near the hot wall. The maximum velocity in the hot wall boundary layer in the partitioned cavity (76.6 mm/s) is much smaller than the corresponding value in the standard cavity (204.0 mm/s), i.e. about 62% down. This is due to the length of the partitions preventing the fluid flow getting to the hot wall. On the other hand, the maximum velocity in the cold wall boundary layer in the partitioned cavity (258.3 mm/s) is about 12% higher than the corresponding value in the standard cavity (227.2 mm/s). This is due to the high heat transfer rates from the hot partitioned wall into the cavity. This higher heat input in the partitioned cavity leads to higher buoyancy force as the fluid flows from the hot wall to the cold wall and as such the fluid flows relatively faster along the cold wall in the partitioned cavity than in the standard cavity. Also, the higher heat input from the hot partitioned wall affects the thickness of the boundary layer especially along the cold wall in the partitioned cavity, i.e. since the fluid particles in the cold wall boundary layer of the partitioned cavity have more energy than the corresponding particles in the standard cavity, they can travel further away from the wall before losing their energy (see Fig. 4).

3.2. Wall shear stress

The flow in the present cavity is limited in the boundary layers along the walls and partitions (see Fig. 3). The velocity profile in the viscous layer is used to determine the wall shear stress. In the viscous layer the velocity profile is a cubic function of distance from the wall (Ampofo, 2001) i.e.

$$\bar{v} = ax + bx^2 + cx^3 \tag{6}$$

where a, b and c can vary depending on height. Then the wall shear stress can be expressed as

$$\tau_w = \mu \left.\frac{\partial \bar{v}}{\partial x}\right|_{x=0} = a \tag{7}$$

Using the measured results in the viscous layer (about 13 measuring points were used in this layer) and a cubic polynomial least squares fitting process, an equation was obtained for the velocity profile. The equation was differentiated at $X = 0$ and 1 to obtain the velocity gradient and then the wall shear stress. The results are shown in Fig. 5. The disagreement of the shear stress values between the two isothermal walls is obvious. This is due to the partitions "preventing the fluid layer reaching" the hot wall. The wall shear stress in both the partitioned and standard cavities is also compared in Fig. 5. The distribution of the wall shear stress in the partitioned cavity is quite interesting. Along the cold wall, the distribution agrees very well with that in the standard cavity but along the hot wall they differ substantially. While the peak value along the hot wall in the standard cavity occurs at $Y = 0.4$, the corresponding value in the partitioned cavity occurs around $Y = 0.1$. Also, the partitions slow down the fluid layer reaching the hot wall and as such the values along the hot wall in the partition cavity are much smaller than the corresponding values in the standard cavity.

3.3. Velocity fluctuation profiles

The vertical velocity fluctuations, v'_{rms}, and the horizontal velocity fluctuation, u'_{rms}, in the partitioned cavity at $Y = 0.587$ are concentrated in the boundary layer and decrease to almost nothing outside the boundary layer (see Fig. 6(a) and (b)). One feature shown in the figures is the difference between u'_{rms} and v'_{rms}. The value of u'_{rms} is less than half that of v'_{rms} in the boundary layer. Fig. 6(a)

also shows that the vertical velocity fluctuation dominates near the isothermal walls and around the tip of the partitions. The v'_{rms} profile at $Y = 0.587$ in the partitioned cavity is compared with that in the standard cavity at $Y = 0.600$ in Fig. 6(a). As expected, the v'_{rms} profile in the hot side of the partitioned cavity is totally different to the corresponding profile in the standard cavity. The profile in the partitioned cavity has three peaks (one low peak in the hot wall boundary layer and two almost comparable peaks around the tip of the partitions and in the cold wall boundary layer) and that in the standard cavity has two (one each in the boundary layers along the isothermal walls). Also, the v'_{rms} profile in the cold wall boundary layer of the partitioned cavity has a much higher peak and a thicker boundary layer. All these are due to the higher heat input from the hot partitioned wall as discussed earlier. Fig. 6(b) shows the comparison of the u'_{rms} profile at $Y = 0.587$ in the partitioned cavity with that in the standard cavity at $Y = 0.600$. Unlike in the standard cavity, the u'_{rms} profile in the partitioned cavity has its peak around the tip of the partitions. Also, due to the higher heat input from the hot partitioned wall, the u'_{rms} profile in the partitioned cavity has a higher peak and thicker boundary layer along the cold wall than the corresponding profile in the standard cavity.

3.4. Mean temperature profiles

As stated earlier, the two isothermal walls were kept at 50 and 10 °C at all times while the horizontal walls were built to be highly conducting. The boundary conditions on the horizontal walls strongly affect the thermal field in the cavity. These conditions are frequently assumed to be adiabatic or perfectly conducting in numerical studies but it is very difficult to achieve such boundary conditions in experimental studies. In Fig. 7, the measured mean temperature profiles on the horizontal walls in both the standard and partitioned cavities are compared. Also in the figure is the profile for the ideal perfectly conducting walls, which give a linear temperature profile (LTP). From Fig. 7, it can be seen that there is not much difference between the temperature profiles on the top wall in the standard and partitioned cavities but the difference between the profiles on the bottom wall is obvious. These temperature profiles, representing real boundary conditions, are recommended for numerical modelling.

A contour plot of the thermal field across the whole of the partitioned cavity is shown in Fig. 8. This is based on all the experimental data. The data was inserted into a 52×98 mesh. It can be seen that between every two successive partitions the boundary layer thickness on the

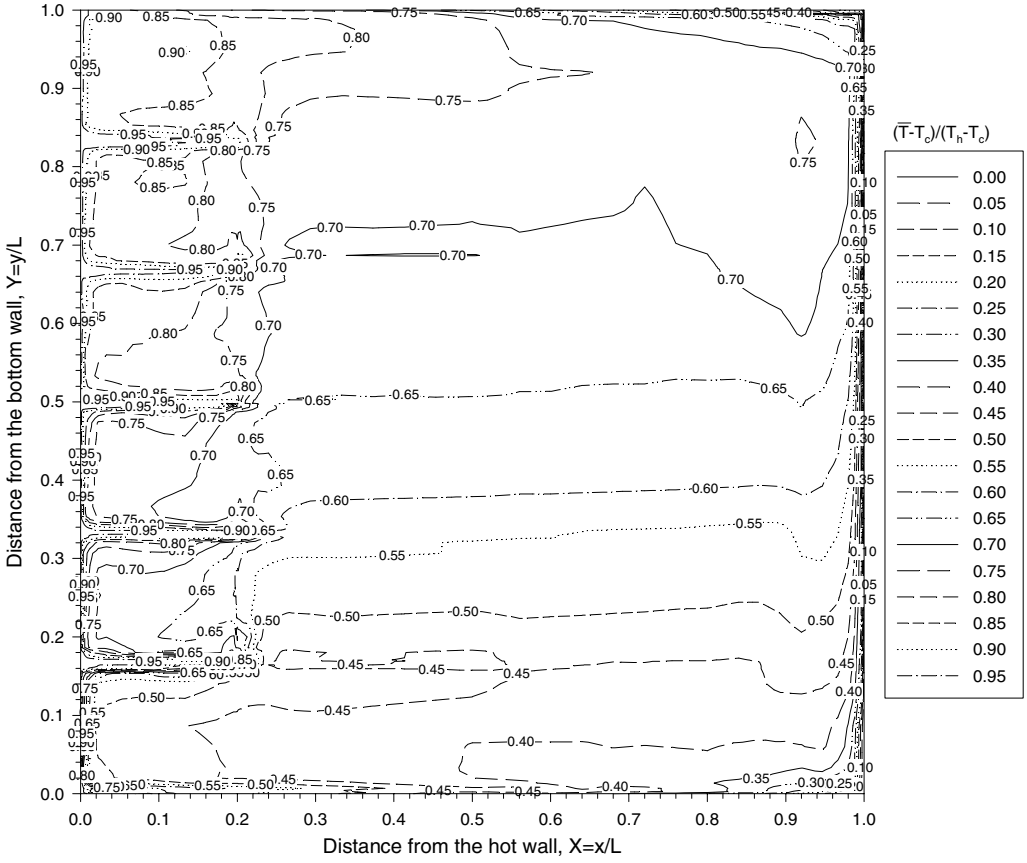

Fig. 8. Contour plot of temperature profile, $(\overline{T} - T_c)/(T_h - T_c)$, in the partitioned cavity.

hot wall increased with the fluid flow as expected. From Fig. 8, the dimensionless temperature at the core of the whole cavity was 0.65 (36 °C), which is about 20% higher than the mean temperature (and the ambient). The effect of this in terms of the heat lost through the passive vertical walls was minimal.

3.5. Temperature fluctuation profiles

The temperature fluctuation, T'_{rms}, profile at $Y = 0.587$ in the partitioned cavity is shown in Fig. 9. As seen in Fig. 9, the temperature fluctuation intensity increases with distance from the wall to a peak and then decreases to almost nothing but near the hot wall, the fluctuation intensity increases again reaching its highest peak around the tip of the partitions. This is due to the higher level of rotational motion of the fluid around the tip of the partitions. The maximum value of the temperature fluctuation intensity in the whole partitioned cavity was around $T'_{\mathrm{rms}} = 4.1$ K at $X = 0.205$ and $Y = 0.187$. Away from the partitions ($X \sim 0.3$ to 0.9), the temperature fluctuation intensity remained constant, indicating that the fluid in this region of the cavity was nearly stationary. The T'_{rms} profile at $Y = 0.587$ in the partitioned cavity is also compared with the corresponding profile in the standard cavity at $Y = 0.600$ in Fig. 9. The T'_{rms} profile in the cold wall boundary layer of the standard cavity agrees very well with the corresponding profile in the partitioned cavity but there is a difference in the hot wall boundary layer. This is in line with the findings of the velocity field.

3.6. Heat transfer

The local and average Nusselt numbers on the hot, cold, bottom and top walls can be determined using the measured temperature data in the thermal conductive

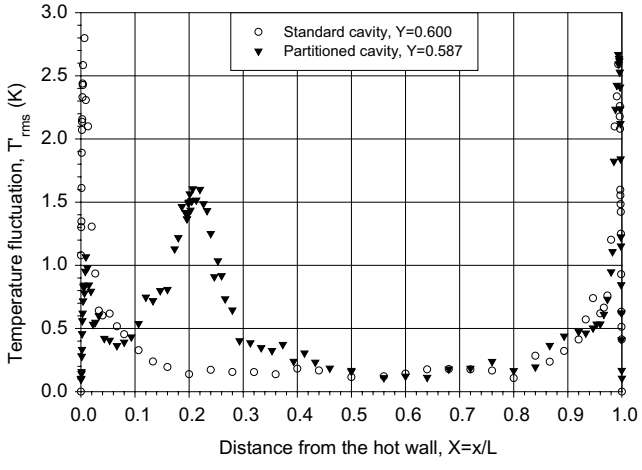

Fig. 9. Temperature fluctuation profile around mid-height.

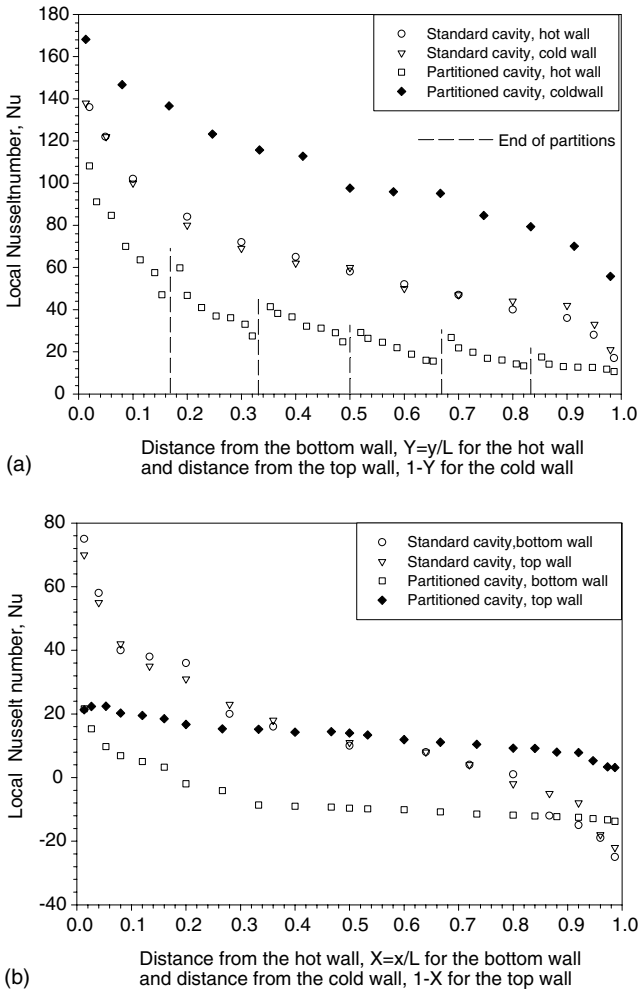

Fig. 10. Local Nusselt number profiles. (a) Local Nusselt number along the isothermal walls and (b) local Nusselt number along the horizontal walls.

boundary layer where the heat flux is constant as follows:

$$Nu_{\mathrm{local}} = -\frac{L}{T_{\mathrm{h}} - T_{\mathrm{c}}} \left.\frac{\partial \overline{T}}{\partial x_i}\right|_{\mathrm{w}} \tag{8}$$

From this definition, the heat flux is positive with axis direction, i.e. the heat transfer from the hot wall into the cavity and from the cavity into the cold wall is positive. The heat transfer from the bottom wall into the cavity and from the cavity into the top wall is positive. The temperature gradient with respect to x or y was estimated by a linear best fitting from the first 6–9 measuring points near the wall. The local Nusselt number on the hot and cold walls of the partitioned cavity is shown in Fig. 10(a). The local Nusselt number reaches a maximum at the bottom of the hot wall and at the top of the cold wall because of thinner thermal boundary there. The measured maximum Nusselt number value is about 110 and 168 for the hot and cold walls respectively. The thickness of the boundary layer is increasing along the

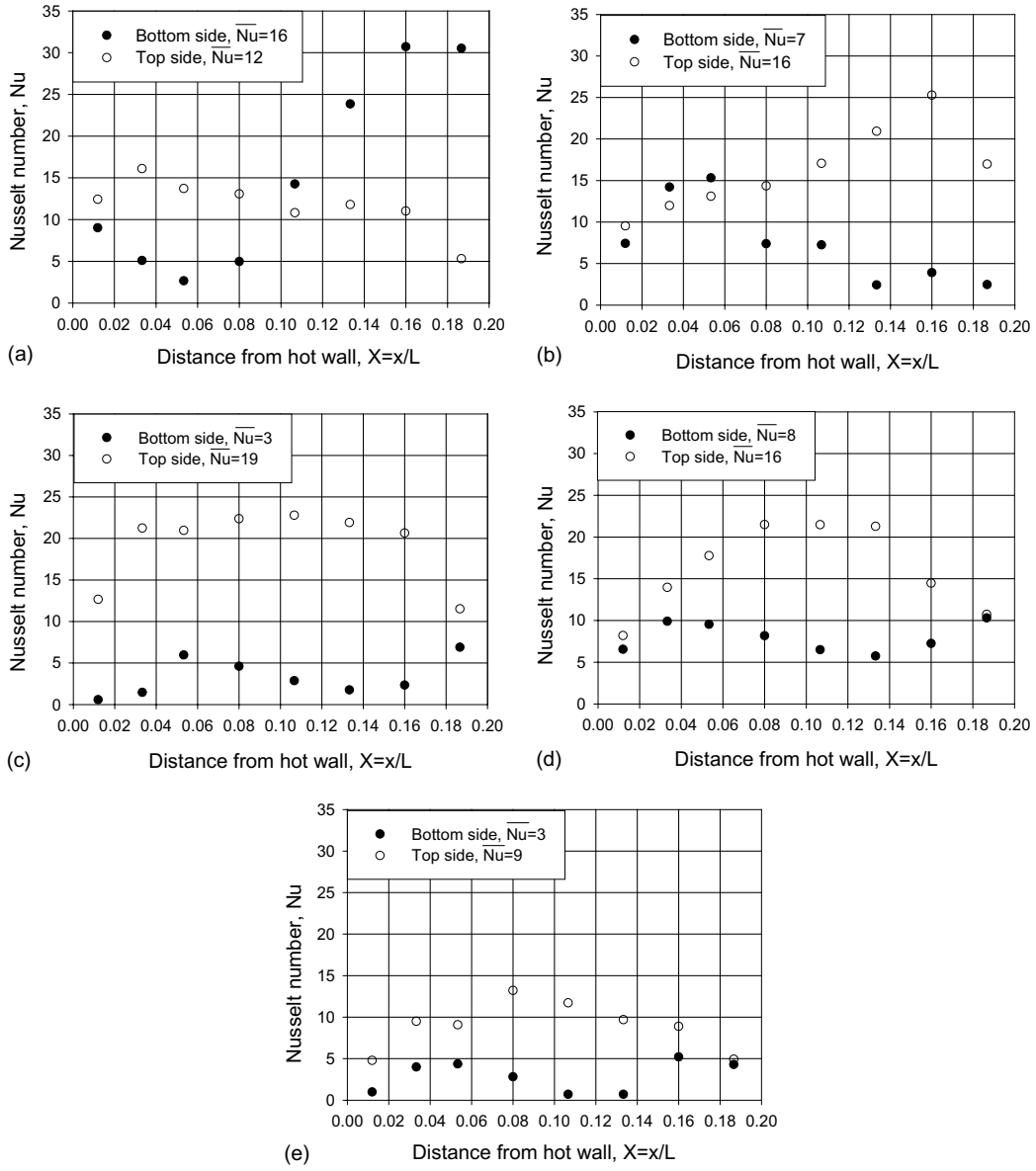

Fig. 11. The local and average Nusselt numbers along the partitions. Partitions at $Y = 0.1667$ (a), $Y = 0.3333$ (b), $Y = 0.5000$ (c), $Y = 0.6667$ (d), and $Y = 0.8333$ (e).

flow direction so that the local Nusselt number decreases rapidly. The Nusselt number distribution in-between partitions was similar in shape to that obtained in a standard cavity with a maximum value near the upper surface of a partition and a reduction to a minimum near the bottom of the next partition. At mid-height, the local Nusselt number is about 25 and 97 for the hot and cold walls respectively. At the other end, because the fluid flow meets the wall, the heat transfer diminishes significantly and the local Nusselt number drops to about 10 and 55 for the hot and cold walls respectively. The average Nusselt number was 34 and 105 for the hot and cold walls respectively. The huge difference for the two sides is accounted for by the partitions on the hot wall. The local Nusselt number on the bottom and top walls of the partitioned cavity is shown in Fig. 10(b). On one part of the bottom wall ($X = 0$–0.184) the heat is transferred from the wall into the cavity and on the other part ($X = 0.184$–1) the heat is transferred from the cavity into the wall whereas over the whole surface of the top wall, the heat is transferred from the wall into the cavity. The average Nusselt number was 6 and 13 for the bottom and top walls respectively but the local Nusselt number can be up to 21. The heat transfer through the bottom and top walls was not significantly high.

The local Nusselt number on the hot and cold walls in the partitioned cavity is compared with the corresponding profile in the standard cavity in Fig. 10(a). As stated earlier, the average Nusselt numbers were 34 and

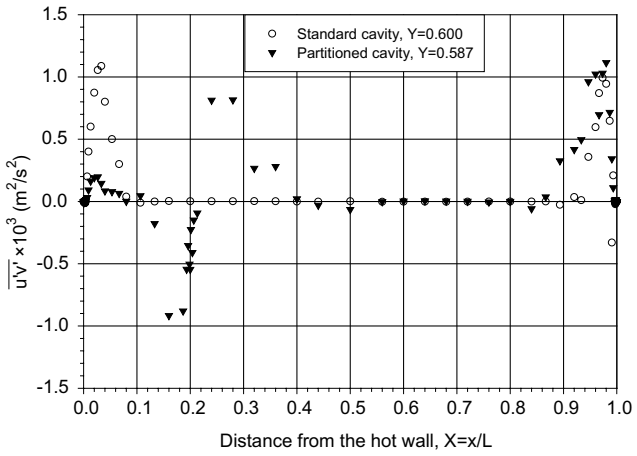

Fig. 12. Reynolds stress profile around mid-height.

105 for the hot and cold walls respectively in the partitioned cavity while the corresponding values in the standard cavity were 62.9 and 62.6 respectively. That is, the partitioned cavity offered a lower heat transfer rate along the hot wall and a higher heat transfer rate along the cold wall as compared to the standard cavity with the same dimensions and under the same experimental conditions. However, in the partitioned cavity, the heat transfer from both the hot wall and the partitions was about 199 W while that for the hot wall in the standard cavity was about 98 W. In Fig. 10(b), the local Nusselt number on the horizontal walls in both the partitioned and standard cavities is compared. Compared to the standard cavity with the same dimensions and under the same experimental conditions the partitioned cavity offered lower heat transfer rate along the bottom and top walls. The average Nusselt numbers were 6 and 13 for the bottom and top walls respectively in the partitioned cavity while the corresponding values in the standard cavity were 13.9 and 14.4 respectively.

Fig. 11 shows the local and average Nusselt number on the partitions. All the partitions transferred heat from their surfaces into the cavity but the amount of heat transferred varied from partition to partition. Considering the huge difference between the average Nusselt number for the hot and cold walls, the heat transfer through the partitions was significantly high. As stated at the end of Section 2, the heat transfer into the cavity from the hot wall together with the partitions was 199.03 W while the net loss from the cold, bottom and top walls was 165.08, 9.88 and 20.81 W respectively. The percentage error of heat input and output in the whole cavity was 1.64%.

3.7. Reynolds stress

The Reynolds stress, $\overline{u'v'}$, profile in the partitioned cavity at $Y = 0.587$ is shown in Fig. 12. The distribution of $\overline{u'v'}$ changes significantly with height along the cold wall and around the tip of the partitions. Fig. 12 confirms that the development of turbulence in the flow in the partitioned cavity is limited in the boundary layer along the cold wall and around the tip of the partitions. The $\overline{u'v'}$ is near zero between $X = 0.4$ and 0.9 across the partitioned cavity. In Fig. 12, the $\overline{u'v'}$ at $Y = 0.587$ in the partitioned cavity is also compared with that in the standard cavity at $Y = 0.600$. The profile of $\overline{u'v'}$ in the partitioned cavity is interesting. Near the cold wall, it is similar to that in the standard cavity with a small increase in the magnitude of the peak value. However, near the hot wall, it has two major peaks (one just before and the other just after the tip of the partitions) and a small peak near the hot wall. The standard cavity exhibits one peak near the hot wall, i.e. similar to the cold wall.

4. Conclusions

The most important conclusion, which can be drawn from the above comparison and discussion, is the effect of the partitions on the heat transfer rates along the hot wall. The local and average *Nu* number was obtained and indicated that partitions of this length tend to reduce the heat transfer rates along the hot wall compared with similar cavities without partitions. On the whole, the velocity field, the temperature field and the turbulence quantities results obtained in the partitioned cavity differ substantially from the corresponding results in the standard cavity with the same dimensions and under the same experimental conditions. Also, due to the high heat transfer input from the hot partitioned wall, all the flow and thermal fields quantities including the turbulence quantities obtained in the cold wall boundary layer of the partitioned cavity have higher peaks and thicker boundary layer structure than the corresponding values in the standard cavity.

The results described in this paper were obtained with high precision and can be useful as benchmark data for comparison with CFD codes. Such numerical simulation should include realistic boundary conditions at the top and bottom horizontal walls as given in this study.

References

Ampofo, F., 2001. Turbulent natural convection in an air filled standard or partitioned square cavity. PhD Thesis, London South Bank University.

Mergui, S., Penot, F., 1996. Natural convection in a differentially heated square cavity: experimental investigation at $Ra_H = 1.69 \times 10^9$. Int. J. Heat Mass Transfer 39 (3), 563–574.

Nansteel, M.W., Grief, R., 1984. Natural convection in enclosures with two- and three-dimensional partitions. Int. J. Heat Mass Transfer 27 (4), 561–571.

Olson, D.A., Glicksman, L.R., Ferm, H.M., 1990. Steady-state natural convection in empty and partitioned enclosures at high Rayleigh numbers. ASME J. HT 112, 640–647.

Penot, F., N'Dame, A., 1992. Successive bifurcations of natural convection in a vertical enclosure heated from the side. In: Heat Transfer, Third UK National Conference Incorporating First European Conference on Thermal Sciences, vol. 1. Birmingham, UK, pp. 507–513.